Scripta Materialia 187 (2020) 360–365

Contents lists available at ScienceDirect

Scripta Materialia

journal homepage: www.elsevier.com/locate/scriptamat

Statistical nature of the incipient plasticity in amorphous alloys

Shankha Nag[a], R.L. Narayan[b], Jae-il Jang[c], C. Mukhopadhyay[d], Upadrasta Ramamurty[e,*]

[a] School of Mechanical Engineering, École Polytechnique Fédérale de Lausanne, Lausanne CH-1015, Switzerland
[b] Department of Materials Science and Engineering, Indian Institute of Technology, Delhi 110016, India
[c] Division of Materials Science and Engineering, Hanyang University, Seoul 04763, South Korea
[d] Department of Management Studies, Indian Institute of Science, Bangalore 560012, India
[e] School of Mechanical and Aerospace Engineering, Nanyang Technological University, Singapore 639798, Singapore

ARTICLE INFO

Article history:
Received 23 May 2020
Revised 19 June 2020
Accepted 19 June 2020
Available online 29 June 2020

Keywords:
Metallic glass
Plastic deformation
Nanoindentation
Statistics
Bimodal distribution

ABSTRACT

Statistical analyses of the first pop-in stress data, obtained by spherical tip-nanoindentation experiments on different metallic glasses (MGs) with tip radius, R_i, loading rate, $\dot{P}$, and structural state of the glass as experimental variables, show that the 3-parameter bimodal Weibull distribution best captures the stochastic nature of the incipient plastic strengths. Significant bimodality in the strength distributions was observed only when a larger R_i and $\dot{P}$ are employed. We hypothesize that the stress required for shear band nucleation has to exceed a critical value over a characteristic distance over which the stress gradients are minimum to rationalize the bimodality.

The shear yield strength, τ_y, of a material can be estimated using the load, P_{FP}, at which first pop-in (FP) occurs during spherical-tip nanoindentation, as [1,2]:

$$\tau_y = 0.17 \left(\frac{1}{R_i}\right)^{2/3} \left(\frac{1-\nu_s^2}{E_s} + \frac{1-\nu_i^2}{E_i}\right)^{-(2/3)} (P_{FP})^{1/3} \quad (1)$$

where R_i is the indenter radius, and E and ν are elastic moduli and Poisson's ratios (subscripts 's' and 'i' denote sample and the indenter, respectively). The variability in τ_y of a metallic glass (MG) reflects the stochastic aspects of incipient plasticity [3–8], due to the intrinsic randomness in their atomic packing. Statistics of τ_y for a variety of MGs were reported and analyzed [9–13]. Perepezko et al. [14] observed that the datasets obtained on four different MGs are bimodal, on which basis they assert the existence of two distinct intrinsic defect sites that trigger the formation of an incipient shear band (SB). However, all their data was obtained with only one R_i (= 5 μm), which means that the probed material's volume is fixed. Moreover, they performed the analyses using the Gaussian distribution function. However, the Weibull statistics have been used to describe the τ_y dispersions [11] as well as size-effects, especially at nanometer-submicron scales [12,13] to show that, in general, their applicability is limited because it does not distinguish between processes like nucleation, propagation and overlap of stress fields. In this work, evaluation of uni- and bimodal versions of three different statistical models was performed on 13 datasets that are generated using wider combinations of experimental variables so as to ascertain the true statistical nature of the incipient plasticity in MGs.

Table 1 summarizes the examined datasets generated on two different Zr-based MGs at room temperature in both as-cast (AC) and structurally relaxed (SR) states. The latter were obtained by annealing MG samples below their T_g. Datasets AC1-AC5 and SR1 were taken from refs. [4,5] whereas AC6, AC7, A1-A4 and SR2 are new. For these, nanoindentation experiments were performed on mirror-polished (using 0.2 μm diamond suspension and kerosene medium) specimens using a Hysitron Triboindeter (R_i = 1 μm).

Statistical analyses of τ_y data were performed using Gaussian, Lognormal, and Weibull models. Both two- and three- parameter versions of the latter (abbreviated as 2 W and 3 W, respectively) were considered. Equations that describe the probability density functions (PDFs) for all the different models are given in the supplementary information (SI). The sample size optimization tests (see S1.1 in SI for the procedure employed) show that a sample size, varying in the range of 100 to 140, is sufficient for making reliable statistical inferences for all the datasets.

The Maximum Likelihood Estimates (MLEs) are consistent with a certain rate of convergence, which depends on the regularity conditions of the assumed model [15]. For the bimodal distributions, we employed the Expectation-Maximization Algorithm (EMA) to obtain the MLEs. (See Section S1.1 of SI for details.) Then,

* Corresponding author.
E-mail address: uram@ntu.edu.sg (U. Ramamurty).

https://doi.org/10.1016/j.scriptamat.2020.06.045
1359-6462/

Table 1
Summary of the different metallic glass (MG) alloy compositions and their structural states, indentation parameters utilized in this study. Datasets AC1 – AC5 and SR1 are taken from Refs. [4,5] whereas the rest were produced for this study.

Dataset	Composition	Thermal history	$\dot{P}$ (mN/s)	R_i (μm)	Data size
AC1	$Zr_{52.5}Cu_{17.9}Ni_{14.6}Al_{10}Ti_5$ (glass transition temperature, T_g = 578 K)	as cast	1	31.5	110
AC2	"	as cast	5	31.5	111
AC3	"	as cast	10	31.5	112
AC4	"	as cast	20	31.5	133
AC5	"	as cast	1	5.75	135
AC6	$Zr_{35}Ti_{30}Cu_{8.25}Be_{26.75}$ (T_g = 673 K)	as cast	0.4	1	100
AC7	"	as cast	0.4	1	100
A1	"	Annealed, 553 K, 520 min	0.4	1	100
A2	"	Annealed, 573 K, 170 min	0.4	1	100
A3	"	Annealed, 593 K, 41 min	0.4	1	100
A4	"	Annealed, 613 K, 15 min	0.4	1	100
SR1	$Zr_{52.5}Cu_{17.9}Ni_{14.6}Al_{10}Ti_5$	Annealed, 630 K, 60 min	1	5.75	112
SR2	$Zr_{35}Ti_{30}Cu_{8.25}Be_{26.75}$	Annealed, 558 K, 1440 min	0.4	1	100

Table 2
Akaike information criterion (AIC) estimates. The estimates marked in bold are the minimum ones among all competing models for the respective dataset. 2 W and 3 W refer to two and three parameter Weibull distributions respectively, whereas G and LN refer to Gaussian and lognormal distributions.

Dataset	Bimodal distribution				Unimodal distribution			
	2W	3W	G	LN	2W	3W	G	LN
AC1	9.8	**−3.0**	−0.2	−1.5	33.5	2.4	21.2	14.7
AC2	28.5	22.9	23.1	**22.1**	51.6	42.0	46.8	45.4
AC3	83.2	**61.8**	75.8	72.8	112.9	77.3	104.4	96.4
AC4	95.5	**89.0**	92.1	92.0	143.0	123.6	139.9	137.3
AC5	63.6	**54.5**	61.4	61.8	76.6	60.7	63.9	61.5
AC6	122.2	**107.1**	117.2	116.9	131.8	113.2	120.1	116.5
AC7	107.2	**100.0**	104.6	103.9	118.7	101.4	107.4	103.0
A1	117.2	**101.0**	109.6	108.8	134.9	103.5	119.3	112.4
A2	137	**122.7**	132.0	128.3	151.2	126.8	138.6	132.3
A3	140.1	**133.9**	140.3	138.0	142.0	136.7	136.2	137.2
A4	142.4	**128.1**	139.3	138.6	150.7	133.1	139.0	134.9
SR1	−32.3	**−63.8**	−40.1	−41.0	−8.5	−46.9	−36.3	−40.6
SR2	194.2	**181.9**	190.2	189.2	198.6	184.8	188.6	185.4

Akaike information criterion (AIC) [16] was utilized to assess the suitability of a selected model to describe the data. The model that yields the lowest AIC value for a given dataset best describes it. On this basis, it is evident from Table 2 that the bimodal 3 W distribution is best suited to describe the stochastic nature of τ_y in MGs. (The exception of the dataset AC2, for which AIC of 3 W is the second lowest.)

Table 3 lists MLEs of the proportions of bimodal components for the 13 datasets. It reveals that both the components are significant only for AC1 to AC4 datasets. In the rest, the second components vary between 1 and 9%. Since these are within the experimental errors and/or sampling noise, it is reasonable to assume that the unimodal 3 W distribution effectively represents the stochastic nature of τ_y in those nine datasets. The Kernel Density Estimates (KDEs) displayed Fig. 1 are in agreement.

The p-values of the Kolmogorov-Smirnov goodness-of-fit tests for the uni- and bi-modal 3W distributions were found using the 'bootstrap' expansion [17]. (See Section S2.3 in SI for details.) For both the distributions, the obtained p-values that are listed in Table 3 are more than the chosen value of the significance level (α_s ~0.05[1]) for all the sets of data. This implies that neither model can be rejected if they are considered only on the basis of goodness-of-fit.

The strength variability in brittle materials is best described by Weibull statistics because the largest defect, which initiates failure, constitutes the weakest link. For MGs, the weakest links can be thought as those local regions where the atomic packing fraction is the lowest, and hence yield first [18–20]. The random nature of the packing also implies spatial heterogeneity in yield strength of the amorphous alloys. Therefore, 3 W model being the best descriptor of the τ_y data of MGs appears physically meaningful.

The Weibull modulus, m, which defines the extent of scatter in the data, ranges between 1.5 and 2.5 for most of the datasets (Table 3). A comparison of it with those obtained from bulk compression tests (m ~ 6) [21,22] and tension tests (m ~ 36) [23] reported in literature suggests that the scatter in τ_y is significantly higher than that of the fracture strength, although both are understood to be mediated by SBs [24,25]. This is similar to that seen in the tensile strength distributions of continuous fiber-reinforced composites where the breakage of the individual fiber exhibit a small m whereas the macroscopic composite failure, which is also statistical in nature, tends to have significantly larger m [26,27]. This is because the failure of fiber composites is driven by the accumulation of broken fiber clusters until one such cluster becomes unstable, which is analogous to the localization of plastic flow in MGs via SB nucleation that has origins in collective cascading of shear transformation zones (STZs) [28–30].

Table 1 shows that AC1–AC4 datasets produced with a large indenter (R_i = 31.5 μm) but with varying $\dot{P}$ are distinctly bimodal. Amongst these, an increase in $\dot{P}$ leads to (a) a shift in the τ_y distribution to higher values, and (b) an enhanced prominence of the bimodal nature. These observations suggest that a larger R_i and/or $\dot{P}$ impart bimodality to τ_y distributions. An examination

[1] Except for the p-value of unimodal Weibull model for dataset AC4; however, the model has already been discarded by AIC.

Table 3
Maximum likelihood estimates (MLEs) along with the p-values of the KS test for unimodal and bimodal 3-parameter Weibull (3 W) distributions. The cells colored green are the relevant parameters for a given dataset: Bimodal distribution is favored for datasets AC1 – AC4 whereas unimodal distribution best describes the rest.

Dataset	3 W bimodal					3 W unimodal			
	Proportion	α	β	m	p-value	α	β	m	p-value
AC1	0.65	1.38	0.29	1.87	1.00	1.38	0.46	1.60	0.51
	0.35	1.87	0.26	1.73					
AC2	0.81	1.43	0.59	2.41	0.91	1.43	0.70	2.26	0.43
	0.19	2.33	0.16	3.26					
AC3	0.76	1.65	0.42	1.48	0.98	1.65	0.60	1.40	0.50
	0.24	1.65	1.13	8.77					
AC4	0.49	1.69	0.30	1.73	0.88	1.68	0.71	1.53	0.04
	0.51	1.70	1.06	5.22					
AC5	0.95	1.68	0.76	2.33	0.99	1.65	0.79	2.51	0.92
	0.05	2.18	0.05	22.62					
AC6	0.94	2.66	0.90	2.03	0.97	2.65	0.95	2.04	0.92
	0.06	3.85	0.32	31.54					
AC7	0.03	2.16	0.01	1.01	0.99	2.08	0.91	2.10	0.98
	0.97	2.24	0.76	1.77					
A1	0.98	2.56	0.75	1.59	0.99	2.56	0.77	1.61	0.98
	0.02	3.78	6E-04	1.00					
A2	0.91	2.43	0.85	1.58	0.82	2.41	0.91	1.74	0.95
	0.09	3.47	0.03	1.00					
A3	0.99	1.99	1.48	3.18	0.91	2.02	1.46	3.04	0.90
	0.01	4.40	1E-04	1.00					
A4	0.98	2.53	1.06	2.04	0.98	2.53	1.07	2.09	1.00
	0.02	3.61	2E-04	2.17					
SR1	0.97	2.65	0.43	1.93	1.00	2.65	0.43	1.96	0.97
	0.03	3.06	3E-05	1.00					
SR2	0.97	2.80	1.44	2.22	0.92	2.79	1.48	2.29	0.96
	0.03	4.72	2E-03	1.00					

of the published literature appears to agree. For example, the bimodal distributions reported by Perepezko et al. [14] are obtained with a relatively large R_i (~5 μm) and a high $\dot{P}$ (20 μN/s). Similarly, Zhao et al. [9] report bimodal τ_y distributions in eight different MGs measured with $R_i = 2$ μm and $\dot{P}$ ranging between 1.1 and 4.56 μN/s. Indentations performed with a single indenter of R_i (=2.5 μm) but with $\dot{P}$ ranging from 0.05 to 2 mN/s by Wang and Perepezko [31] show that the bimodal nature gets increasingly prominent at higher $\dot{P}$. Additionally, it appears that the structural state of MG influences the τ_y distribution as well, as seen in Fig. 1(b). Structural relaxation of the MG moves the τ_y distribution to higher stresses, which is consistent with that reported by Perepezko et al. on a Fe-based MG [14].

The fact that both R_i and $\dot{P}$ are experimental variables suggests that the observed bimodal distributions manifest only under specific experimental conditions. This raises the following issues. If the bimodal distribution is indeed due to the presence of more than one kind of 'defect', as hypothesized by Perepezko et al. [14,31], one would rather expect unimodal distribution in τ_y for large R_i and a bimodal distribution for smaller R_i. This is because with an increasing R_i, the volume of the material that is being probed increases cubically, which results in a higher probability of finding both kinds of defects in the probed volume in every indentation. Since the weakest defects must always be the ones to get activated first, a unimodal distribution should result when a large indenter is used. Therefore, an alternative mechanistic rationale for the observation of bimodal distributions under the aforementioned experimental conditions is necessary.

The activation of a single STZ being the source of the pop-in can be ruled out as the size of it, even if one considers the largest STZ, is orders of magnitude smaller than the volume of the material displaced during the pop-in [32]. On this basis, we infer that the first pop-in is probably linked to the embryonic formation of a SB underneath the indenter.

An approximate estimate of the number of activable STZs that can be found within the volume of the material that is deforming underneath the indenter (See Section S2 of SI for details) that when the MG indented with a large indenter (R_i = 31.5 μm), 388 STZs can potentially get activated whereas only 6 STZs can be accessed during a single indentation when a smaller tip (R_i ~ 5.75 μm) is used. Since the smaller tip has access to lesser number of STZs, higher stress would be essential to form a SB, which rationalizes the observed shift in τ_y distribution to higher values when smaller R_i tips are used. Moreover, the probability of multiple SBs nucleating simultaneously within the deformed volume greatly reduces due to the small number of activable STZs. Therefore, plastic deformation would commence via the linking up of all the activated STZs to form a SB.

With large R_i, multiple sources for SB nucleation getting activated becomes a possibility as a larger volume of MG is probed, resulting in a bimodal τ_y distribution. Since the stress distribution underneath a spherical indenter is complex with strong gradients, one can envision a scenario in which yielding occurring when an embryonic SB of a critical length is nucleated [33], which, in turn, requires some minimum number of STZs to be activated along the shearing plane. Importantly, a sustainable SB can only nucleate if the shear stress along any contour is higher than the stress required to activate STZs at several locations on it. Consequently, initiation of plastic deformation is most favored only along the contour that sustains a sufficiently large value of stress over a significant portion of its length. In essence, the above criterion is analogous to the Ritchie-Knott-Rice fracture criterion in brittle materials which states that crack begins to propagate when the normal stress exceeds a critical value over at a certain distance ahead of the crack tip [34–37].

The above hypothesis is illustrated using Fig. 2(a), in which the variations of the Mohr-Coulomb flow stress, τ_{MC} (= $\tau + \eta\sigma_m$, where τ is the shear stress, η is the coefficient of internal friction ($\approx$ 0.13 [38]) and σ_m is the hydrostatic stress [39]) along four

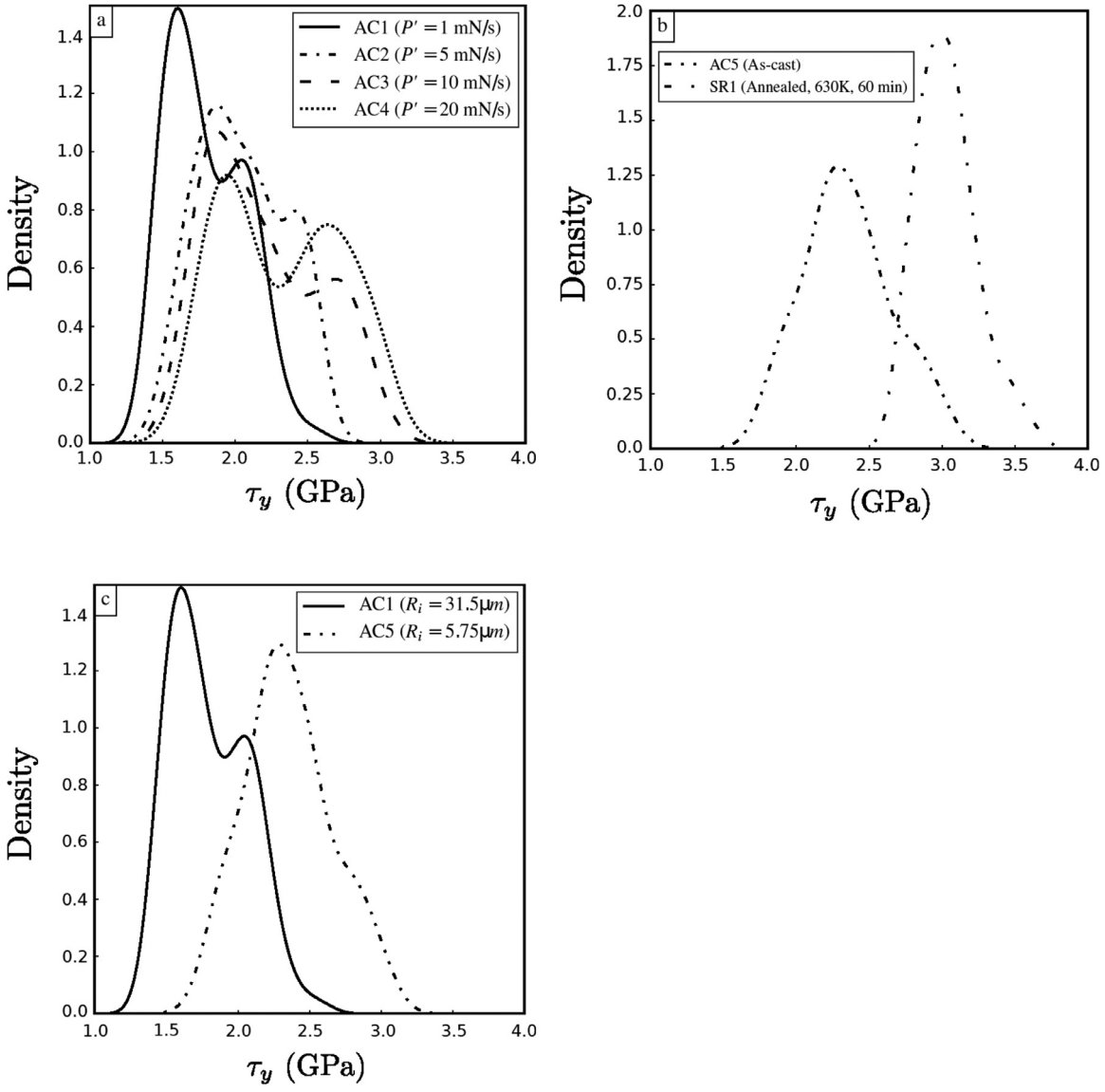

Fig. 1. Strength distribution represented as KDE of τ_y in different MGs demonstrating the individual effects of (a) loading rate, $\dot{P}$ (b) alloy thermal history and (c) indenter tip radius, R_i.

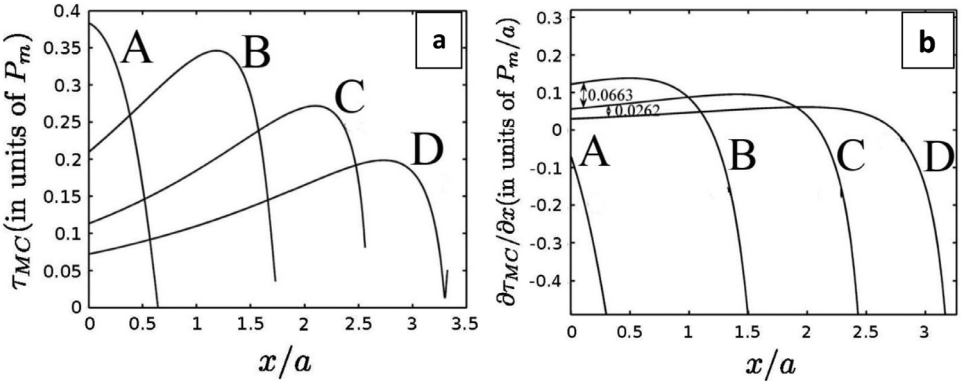

Fig. 2. (a) Variations of τ_{MC} in space (b) gradients in τ_{MC} along the length of four discrete spacial contours. x varies from r' = 0 to z' = 0 (See S2 in SI).

discrete potential SB trajectories (See Fig. S4 in SI for these trajectories) are plotted as a function of x/a, the distance along each contour (See Section S3 of SI for Hertzian contact relations). As seen, τ_{MC} varies non-monotonically along each trajectory. Due to the stress gradients along each contour, initiation of plasticity will be most favored only along the contour that sustains a sufficiently large value of τ_{MC} that facilitates SB formation [40]. Since the energy barrier for STZ activation is not single valued, but has a large variance [41,42], we suppose that τ_{MC} has to be exceeded over some characteristic length.

The high gradients in the stress field underneath the indenter make it difficult to satisfy the above condition. In Fig. 2(b), variations in the shear stress gradients, $\frac{\partial \tau_{MC}}{\partial x}$, along the four contours, which are displayed in Fig. 2(a), are plotted. On the basis of the estimated variations of τ_{MC} and $\frac{\partial \tau_{MC}}{\partial x}$, nucleation of a SB along contours A (steep $\frac{\partial \tau_{MC}}{\partial x}$) and D (low peak value of τ_{MC}) is not favored. Of the remaining contours, B sustains a higher value of τ_{MC} over a significant part of its length compared to C. However, the former has a significantly high $\frac{\partial \tau_{MC}}{\partial x}$ compared to the latter. Based on these considerations, contour C is the most preferred path for incipient plasticity via SB nucleation [40].

The preferred path for SB nucleation will also be influenced by R_i. This is because $\frac{\partial \tau_{MC}}{\partial x}$ is expressed in terms of P_m/a, which is inversely proportional to R_i. Therefore, when an indenter with larger R_i is used, while the spacial profiles of the τ_{MC} contours remain unaltered, the magnitude of $\frac{\partial \tau_{MC}}{\partial x}$ along each contour reduces. This, in turn, will increase the likelihood of SB nucleation along the previously unfavorable stress contours, such as B. Moreover, indenters with larger R_i access significantly larger number of STZs, which further increases the possibility of SB nucleation along several different competing stress contours. In the following, this observation can be utilized to rationalize the influence of R_i and $\dot{P}$ on the nature of the strength distributions seen in Fig. 1(c).

Datasets AC1–AC4, obtained with a large indenter (R_i ~31.5 μm), exhibit a bimodal distribution of τ_y because a SB can potentially form along several different stress contours. At any given load, however, τ_{MC} along one contour is higher than the other. In such a situation, SB nucleation along the contour with higher τ_{MC} can occur at a lower value of τ_y as compared to that on a contour with lower τ_{MC}. *This difference in the stress required for SB nucleation along different stress trajectories manifests as the bimodal distribution of* τ_y. In contrast, the strength distribution is unimodal when indenters with a smaller R_i are employed because the combination of (a) a relatively small value of $\frac{\partial \tau_{MC}}{\partial x}$ along a particular trajectory and (b) the lower concentration of STZs in the indented volume, make that particular stress trajectory an exclusive path for incipient plasticity. The comparatively lower τ_{MC} along that trajectory also explains the shift in the strength distribution of τ_y to higher values. At higher $\dot{P}$, activation of multiple STZs for rapid stress relaxation requires a longer trajectory for initiating plasticity. As this increases the probability of SB formation along several different stress trajectories, the τ_y distribution becomes bimodal at higher $\dot{P}$.

We now turn to the enhancement in τ_y distribution to higher stresses after structural relaxation, during which the free volume content in MGs decreases markedly [35]. A low free volume content increases the STZ activation stress, and, in turn, makes it difficult for the SB-mediated plasticity to occur [35,43]. Therefore, in the annealed state, the average stress required to nucleate SBs in MGs is higher than that in the as cast state [35–38].

In summary, detailed statistical analyses of the incipient plastic strengths of MGs show that they are best described by a three-parameter bimodal Weibull distribution [44]. The bimodal nature of the distribution is prominent only when either large indenters or high loading rates, or both, were employed. Analyses of the stress distributions and their gradients suggests that the stress required to nucleate a SB along a particular shear trajectory depends on both R_i and $\dot{P}$, when a critical stress has to be exceeded over some characteristic length. For large R_i and $\dot{P}$, several stress trajectories become fertile; the difference in the stress required for SB nucleation among them induces bimodality to τ_y.

Declaration of Competing interest

The authors declare that they have no known competing financial interests or personal relationships that could have appeared to influence the work reported in this paper.

Acknowledgements

This work at NTU was conducted under the Structural Metals and Alloys Programme, which was funded by A*STAR, Singapore. The work at Hanyang University was supported by the National Research Foundation of Korea (NRF) grants funded by the Korea government (MSIT) (No. 2020R1A2B5B01001446 and No. 2020R1A5A6017701).

Supplementary materials

Supplementary material associated with this article can be found, in the online version, at doi:10.1016/j.scriptamat.2020.06.045.

References

[1] A.C. Fischer-Cripps, Introduction to Contact Mechanics, Springer, 2000.
[2] K.L. Johnson, Contact Mechanics, Cambridge University Press, Cambridge, 1985.
[3] C.E. Packard, O. Franke, E.R. Homer, C.A. Schuh, J. Mater. Res. 25 (2010) 2251–2263.
[4] I.-.C. Choi, Y. Zhao, B.-.G. Yoo, Y.-J. Kim, J.-.Y. Suh, U. Ramamurty, J. Jang, Scr. Mater. 66 (2012) 923–926.
[5] I.-.C. Choi, Y. Zhao, Y.-.J. Kim, B.-.G. Yoo, J.-.Y. Suh, U. Ramamurty, J. Jang, Acta Mater 60 (2012) 6862–6868.
[6] C.A. Schuh, A.C. Lund, J. Mater. Res. 19 (2004) 2152–2158.
[7] J.R. Morris, H. Bei, G.M. Pharr, E.P. George, Phys. Rev. Lett. (2011) 106.
[8] R.L. Narayan, P. Tandaiya, G.R. Garrett, M.D. Demetriou, U. Ramamurty, Scr. Mater. 102 (2015) 75–78.
[9] X.N. Zhao, Q.P. Cao, C. Wang, X.D. Wang, D.X. Zhang, S.X. Qu, J.Z. Jiang, J. Non. Cryst. Solids 445–446 (2016) 19–29.
[10] D. Tönnies, K. Samwer, P.M. Derlet, C.A. Volkert, R. Maaß, Appl. Phys. Lett. (2015) 106.
[11] P.M. Derlet, R. Maaß, J. Appl. Phys. 120 (2016) 225101.
[12] J.R. Greer, J.T.M. De Hosson, Prog. Mater. Sci. 56 (2011) 654–724.
[13] C.Q. Chen, Y.T. Pei, J.T.M. De Hosson, Philos. Mag. Lett. (2009).
[14] J.H. Perepezko, S.D. Imhoff, M.-.W. Chen, J. Wang, S. Gonzalez, Proc. Natl. Acad. Sci. USA 111 (2014) 3938–3942.
[15] R. Hogg, J. McKean, A. Craig, Introduction to Mathematical Statistics; Chapter 6, sixth ed., Pearson Education, Upper Saddle River, N.J., 2005.
[16] H. Akaike, IEEE Trans. Autom. Control 19 (1974) 716–723.
[17] C.R. Rao, Linear statistical inference and its applications, 1965.
[18] J. Ding, S. Patinet, M.L. Falk, Y. Cheng, E. Ma, Proc. Natl. Acad. Sci. USA 111 (2014) 14052–14056.
[19] M.C. Li, M.Q. Jiang, G. Ding, Z.H. Peng, F. Jiang, L. He, J. Sun, J. Non Cryst. Solids 468 (2017) 52–57.
[20] P. Tsai, K. Kranjc, K.M. Flores, Acta Mater. 139 (2017) 11–20.
[21] Z. Han, L.C. Tang, J. Xu, Y. Li, Scr. Mater. 61 (2009) 923–926.
[22] Y.-Y.Y. Zhao, E. Ma, J. Xu, Scr. Mater. 58 (2008) 496–499.
[23] J.H. Yao, J.Q. Wang, L. Lu, Y. Li, Appl. Phys. Lett. 92 (2008) 2013–2016.
[24] R. Narasimhan, P. Tandaiya, I. Singh, R.L. Narayan, U. Ramamurty, Int. J. Fract. 191 (2015) 53–75.
[25] R.L. Narayan, D. Raut, U. Ramamurty, Acta Mater. 150 (2018) 69–77.
[26] U. Ramamurty, F.W.W. Zok, F.A.A. Leckie, H.E.E. Dève, Acta Mater. 45 (1997) 4603–4613.
[27] T. Okabe, N. Takeda, Y. Kamoshida, M. Shimizu, W.A. Curtin, Compos. Sci. Technol. 61 (2001) 1773–1787.
[28] E.R. Homer, C.A. Schuh, Acta Mater. 57 (2009) 2823–2833.
[29] M.L. Manning, J.S. Langer, J.M. Carlson, Phys. Rev. E 76 (2007) 056106.
[30] L. Li, E.R. Homer, C.A. Schuh, Acta Mater. 61 (2013) 3347–3359.
[31] J.Q. Wang, J.H. Perepezko, J. Chem. Phys. (2016) 145.
[32] C.A. Schuh, T.G. Nieh, J. Mater. Res. 19 (2004) 46–57.
[33] F. Shimizu, S. Ogata, J. Li, Acta Mater. 54 (2006) 4293–4298.
[34] R.O. Ritchie, J.F. Knott, J.R. Rice, J. Mech. Phys. Solids 21 (1973) 395–410.

[35] P. Tandaiya, R. Narasimhan, U. Ramamurty, Acta Mater. 61 (2013) 1558–1570.
[36] D. Raut, R.L. Narayan, Y. Yokoyama, P. Tandaiya, U. Ramamurty, Acta Mater. 168 (2019) 309–320.
[37] R.L. Narayan, P. Tandaiya, R. Narasimhan, U. Ramamurty, Acta Mater. 80 (2014) 407–420.
[38] V. Keryvin, K.E. Prasad, Y. Gueguen, J.-.C. Sangleboeuf, U. Ramamurty, Phil. Mag. 88 (2008) 1773–1790.
[39] R.W. Hertzberg, Deformation and Fracture Mechanics of Engineering Materials, J. Wiley & Sons, 1996.
[40] C.E. Packard, C.A. Schuh, Acta Mater. 55 (2007) 5348–5358.
[41] P.M. Derlet, R. Maaß, Philos. Mag. 93 (2013) 4232–4263.
[42] P.M. Derlet, R. Maaß, Philos. Mag. 94 (2014) 2776–2803.
[43] P. Murali, U. Ramamurty, Acta Mater. 53 (2005) 1467–1478.
[44] W. Weibull, J. Appl. Mech. (1951) 1–7.